SUPPORTING INFORMATION FOR

Mcl-1 and Bok Transmembrane Domains: Unexpected Players in the Modulation of Apoptosis

Estefanía Lucendo, Mónica Sancho, Fabio Lolicato, Matti Javanainen, Waldemar Kulig, Diego Leiva, Gerard Duart, Vicente Andreu-Fernández, Ismael Mingarro, Mar Orzáez*

*Corresponding author: Mar Orzáez

E-mail: morzaez@cipf.es

This PDF file includes:

Material and Methods

Table S1-S4

Figure Legend S1-S9

Figure S1-S9

Material and Methods

Cell Culture

The HCT116 human colorectal carcinoma cell line was kindly provided by Professors Richard Youle and Bert Vogelstein. Cells were grown in McCoy's 5A medium supplemented with 10% fetal bovine serum (FBS). HeLa mtDsRed cells were kindly provided by Prof. Juan V. Esplugues and grown in DMEM supplemented with 10% FBS. Cell lines were cultured in a humidified atmosphere of 5% CO_2 and air at 37ºC.

Bimolecular Fluorescence Complementation-TMD Assays

Bimolecular fluorescence complementation (BiFC) analysis was performed as previously described (1). An improved BiFC assay with a high signal-to-noise ratio was selected to avoid background interference (2, 3). The Mcl-1, Bcl-2, Bid, Bax, Bak, and Bok TMDs were cloned at the C-terminal end of Venus protein fragments, maintaining their natural topology in full-length proteins. To clone the Bcl-2 TMDs, BiFC plasmids (Addgene, 27097 and 22011) were modified, inserting a linker (GGGGSGGGGSSGR for VN and RPACKIPNDLKQKVMNHDKQKSGR for VC) and NotI restriction site behind the Venus fragment. Bcl TMDs were fused to the Venus VN-terminal (1-155, I152L) and VC-terminal (155-238, A206K) fragments and introduced by oligonucleotide annealing. Mutations of BiFC TMDs were obtained using standard site-directed mutagenesis using the Stratagene Quikchange II kit. HCT116 cells were seeded in six-well plates and co-transfected with 0.5 µg of VN and VC DNA constructs using TurboFect (Thermo Scientific™) according to manufacturer instructions. For Venus fluorescence measurement, cells were harvested and resuspended in 150 µl phosphate-buffered saline (PBS) after 16 h transfection. Fluorescence emission was measured using 96 well black plates and a Wallac 1420 Workstation (ʎexc 510 nm and ʎem 535 nm).

Gel electrophoresis and immunoblotting.

Whole-cell extracts were subjected to SDS-PAGE, transferred to nitrocellulose membranes, and blotted following standard procedures. Membranes were probed with the following primary antibodies: rabbit monoclonal anti-HA (clone Y-11, no. H6908) and rabbit polyclonal anti-Tom20 (clone FL-145, no. 11415) from Santa Cruz; mouse monoclonal anti-c-myc (clone 9B11, no. 2276S), rabbit polyclonal anti-Mcl-1 (no. 4572), rabbit monoclonal anti-Bcl-2 (clone 50E3, no. 2870), rabbit anti-Bcl-xL (clone 54H6, no. 2764) from Cell signaling; rabbit monoclonal [EPR15331] anti-Bok (ab186745) and rat anti-tubulin YL1/2 (ab6160) from Abcam. Secondary antibodies specific for mouse, rabbit or rat IgG conjugated with peroxidase for enhanced chemiluminescence (ECL) detection (Amersham Pharmacia Biotech) were purchased from Sigma-Aldrich. Immunoblot signals were detected using GE Healthcare's ECL detection reagents and acquired in an ECL™ Detection System.

Subcellular Fractionation

A total of $1x10^6$ HCT116 cells were harvested, washed in cold PBS, and resuspended in cold SEM buffer (10 mM HEPES, 250 mM sucrose, pH 7.2) supplemented with a protease inhibitor cocktail (Complete, Roche). Cells were mechanically lysed by passing them through a 23G needle. Nuclei and cellular debris were removed by centrifugation at 500 g for 5 min at 4ºC. The post-nuclear supernatant was centrifuged at 15,000 g for 30 min at 4ºC, and the cytosol (supernatant) and heavy membranes (pellet) fractions were separated. The crude heavy membrane pellet was washed twice in cold SEM buffer and centrifuged at 13,000 g for 5 min at 4 ºC. The resulting pellets were solubilized in Laemmli buffer. The cytosolic fraction was centrifuged at 100,000 g for 1 h at 4ºC, and the supernatant subjected to acetone precipitation for 1 h at -20ºC. After centrifugation, cytosolic pellets were also solubilized in Laemmli buffer. Protein samples were separated on denaturing 12% SDS-PAGE gels and analyzed by Western blotting.

Carbonate Extraction

Crude heavy membranes fractions from HCT116 were prepared as described above, resuspended in 0.1 M cold sodium carbonate solution (pH 11.5), incubated for 20 min on ice and centrifuged at 155,000 g for 35 min at 4ºC. The supernatant (alkali-extractable proteins) was titrated back to pH 7 with Tris buffer and subjected to acetone precipitation as described above. The pellets (alkali-resistant proteins) were solubilized in Laemmli buffer for 5 min at 95ºC, separated on denaturing SDS–PAGE gels and analyzed by Western blotting.

Caspase 3/7 Activity

HCT116 cells were plated in six-well plates at 400,000 cells/well for 24 h. The cells were then transfected with 1 µg total VN plasmid or 0.5 µg VN construct plus 0.5 µg pcDNA3.1 plasmid using TurboFect (Thermo Scientific™), according to manufacturer instructions. After 16 h protein expression, cells were harvested, and the pellets were resuspended in lysis buffer (10.2 mM HEPES pH 7.4, 10 mM KCl, 1 mM EDTA, 1 mM EGTA, 1.5 mM $MgCl_2$ and 1 mM DTT, supplemented with a protease inhibitor cocktail). The pellets were frozen and thawed three times using liquid nitrogen, and cell lysates then centrifuged at 13,200 rpm for 10 min. The supernatants were collected, and total protein concentration was quantified by using the bicinchoninic acid (BCA) method. For caspase 3/7 kinetics, a total of 50 µg protein was mixed with 200 µl caspase assay buffer (PBS, 10% glycerol, and 2 mM DTT) containing 20 µM Ac-DEVD-AFC. Caspase activity was monitored using a Wallac 1420 Workstation (λexc 400 and λem 508 nm).

Confocal Live Cell Imaging

HCT116 or Hela mtDsRed cells were transfected, as previously described, in a microscope cover glass (24 mm diameter) stained with Hoechst for nuclei detection and maintained in DMEM at 37°C and 5% CO_2 for imaging. Image acquisition used a Leica SP8 confocal microscope. Excitation light came from 405 nm, 448 nm, and 552 nm lasers. Pearson's coefficient was calculated using LASX software. Images processing was performed using FiJi software.

TMRE Staining

Cells transfected in the above-described conditions were incubated with 50 nM TMRE dye (Invitrogen, T669) at 37ºC/5% CO_2 for 30 min. Then, samples were analyzed in a CytoFLEX flow cytometer. As a positive control of mitochondrial depolarization, cells pretreated with 20 µM FCCP for 10 min were used.

Lactate Dehydrogenase Activity

Cell viability was analyzed in parallel by evaluating the release of lactate dehydrogenase (LDH) using a commercially available kit (CytoTox-ONE™ Homogeneous Membrane Integrity Assay; Promega). The release of LDH was calculated using the formula: the release of LDH (%) = 100× (Abs490 treated −Abs490 untreated cells) / Abs 490 nm untreated cells lysed with Triton 9% (maximum release of LDH).

Cell Toxicity Assay

Cell viability was measured by a 3-(4,5-dimethylthiazol-2-yl)-5-(3-carboxymethoxyphenyl)-2-(4-sulfophenyl)-2H-tetrazolium (MTS) assay, using the CellTiter 96® Aqueous Non-Radioactive Cell Proliferation Assay kit (Promega). WT, shControl or shBok HCT116 cells were grown in 96-well plates at a cell densitiy of 7,5 x 10^4 cells/well. After 24h, cells were transfected with the indicated plasmids and 16 h later, cell viability MTS assay was performed according to manufacturer instructions. Plates were read at 490 nm on a Wallac 1420 workstation.

Bok Silencing

HCT116 cells were plated in six-well plates at a concentration of 400,000 cells/well. Cells were transfected with the On-Target plus Human Bok siRNA (Dharmacon). Transfection solution (OPTIMEM without supplements) contained 2.5 µl Lipofectamine 2000 (Invitrogen) and 150 µM siRNA. After 24 h, cells were transfected with 1 µg VN plasmids, and cell extracts were processed after 18 h expression.

Immunoprecipitation

1x10^6 HCT116 cells were seeded on 150-mm plates and transfected on the following day with 12 µg VN Mcl-1 plasmid +/- 12 µg pcDNA3.1/Bok plasmid plus the transfection reagent TurboFect (Thermo Scientific™). Immunoprecipitation was performed with a Pierce™ Classic IP Kit (Thermo Scientific™) according to the manufacturer's instructions. Briefly, cells were lysed in 1.5 ml IP Lysis/Wash Buffer for 5 minutes on ice and lysates then cleared by centrifugation. Lysates were next precleared using 80 µl of the Control Agarose Resin slurry for 1 h at 4ºC on a rotating wheel. 500 µg of lysate were added to columns containing 5 µg of immobilized anti-c-myc antibody (9B11, #2276S, Cell signaling), and the mixture was incubated overnight at 4ºC on a rotating wheel. Samples were eluted by centrifugation, and co-immunoprecipitates analyzed by Western blotting.

Mcl-1 Somatic Mutants

Somatic mutations that affect the Mcl-1 TMD were identified using the catalog of somatic mutations in cancer (COSMIC). Mcl-1 full-length mutants were obtained, as mentioned previously for the BiFC TMDs constructs, using the pcDNA3.1/Mcl-1 vector.

Statistical Analysis

All values represent the mean ± S.E.M. of at least three independent experiments. Statistical significance was determined by one-way ANOVA, applying the Dunnett's test, or two-way ANOVA, using Sidak's post-test. $P < 0.05$ was designated as statistically significant. The Graph Pad 8 software was used for statistical analysis.

Sequences of the TMDs of Human Mcl-1, Bcl-2, Bid, Bax, Bak, and Bok Proteins

Mcl-1 and Bok TMDs have been selected based on based on the TMHMM Server v. 2.0 predictions (Krogh A, Larsson B, von Heijne G, Sonnhammer EL. Predicting transmembrane protein topology with a hidden Markov model: application to complete genomes. Journal of Molecular Biology. 2001 Jan;305(3):567-580. DOI: 10.1006/jmbi.2000.4315).

Protein	Accession nº	Amino acid sequence
Mcl-1	Q07820	^{323}DLEGGIRNVLLAFAGVAGVGAGLAYLIR^{350}
Bcl-xL	Q07817	^{203}SRKGQERFNRWFLTGMTVAGVVLLGSLFSRK^{233}
Bid	Q92934	^{144}KEKTMLVLALLLAKKVA^{160}
Bax	Q92934	^{169}TWQTVTIFVAGVLTASLTIWKKMG^{192}
Bak	Q16611	^{188}ILNVLVVLGVVLLGQFVVRRFFKS^{211}
Bok	Q9UMX3	^{184}GRLRSHWLVAALCSFGRFLKAAFFVLLPER^{213}

Molecular Dynamics Simulations

Structural Models

We constructed alpha-helical peptides in atomistic resolution using the on-line ProBuilder tool (https://nova.disfarm.unimi.it/probuilder.htm). For Mcl-1, we used a sequence of ^{328}IRNVLLAFAGVAGVGAGLAYLIR^{350} without additional flanking residues. For Bok and Bax we used the sequences of ^{183}SGRLRSHWLVAALCSFGRFLKAAFFVLLPER^{213} and ^{166}SGRTWQTVTIFVAGVLTASLTIWKKMG^{192}, respectively. For these two peptides, the SGR sequence of flanking residues was used to ensure that the peptides remained within the membrane during simulations. The generated peptides were each embedded in a lipid bilayer using the CHARMM-GUI web portal with GROMACS-compatible outputs (4). The bilayers consisted of a total of 128 1-palmitoyl-2-oleoyl-sn-glycero-3-phosphocholine (POPC) lipids

spread evenly between two bilayer leaflets. The membrane was solvated with 5120 water molecules, corresponding to full hydration at 40 water molecules per lipid. Ions were also added to neutralize the charges in the peptides.

These three membranes were simulated for 1 μs to allow the peptide conformation to relax in the native membrane environment. We used the CHARMM36 force field for lipids (5), the CHARMM36m force field for proteins (6), the CHARMM-specific TIP3P model for the water molecules (7), and the CHARMM ion parameters with the NBFIX correction (8). For this simulation, the suggested CHARMM simulation parameters for GROMACS (4) were used. These parameters are listed in detail later in this document when the final production set of simulations is described.

After the equilibration simulation in atomistic resolution, we transformed the peptide into coarse-grained resolution using the martinize2 tool. We used the pre-launch version of 3.4.17 of the MARTINI model force field (9), which accounts for the excessive aggregation of membrane proteins (10). This version corresponds closely to the final version with small differences in the alanine parametrization.

Coarse-Grained Simulations

A daft-like approach (11) has been employed to sample the dimerization interfaces with low interaction energies. Two peptide monomers were placed 3 nm apart (respect to their centers of mass) and randomly tilted with respect to the membrane normal using the daft.sh script (11). A total of 1000 structures have been generated and embedded in a pre-equilibrated lipid bilayer containing 256 2-dioleoyl-sn-glycero-3-phosphocholine (DOPC) molecules using the approach based on high lateral pressure demonstrated by Javanainen (12). Note that we used DOPC instead of POPC used in atomistic simulations since the pre-launch version of Martini 3 reproduced the properties of unsaturated chains better than those of saturated chains.

The systems were then hydrated with 48 water molecules per lipid (1 CG water bead models 4 water molecules) and a concentration of 0.15 of NaCl was added to mimic physiological conditions. See Table 1 for simulations details.

Table 1. Details on the coarse-grained simulations.

Dimer	# Water Beads	# Na+	# Cl-	Time (μs)	# Repeats
Mcl-1–Mcl-1	3057	32	36	4	1000
Mcl-1–Bok	3059	30	36	4	1000
Mcl-1–Bax	3058	31	36	4	1000
Bok–Bok	3059	29	37	4	1000
Bax–Bax	3059	30	36	4	1000

All the simulations were performed with version 2016.6 of the GROMACS 2016.6 package (13) with the pre-launch version of the Martini 3 model, as described above.

All simulations were performed under the isothermic–isobaric (NpT) ensemble with the time step of 20 fs. The Nosé–Hoover thermostat (14, 15) with a time constant of 1 ps was used to maintain the constant temperature of 310 K. The temperature of the solute (peptides and lipids), and the

solvent (water and ions) were controlled independently. The Parrinello–Rahman barostat (16) with the time constant of 12 ps was utilized to keep the pressure the system at 1 bar. A semi-isotropic scheme was used for pressure control. The Verlet cutoff scheme (17) was employed.

The electrostatic interactions were calculated using the reaction-field method with a cutoff at 1.1 nm. The electrostatic interactions within the cut-off radius were handled with a relative dielectric constant of 15 switching to infinite beyond the cut-off radius (18). The Lennard-Jones interactions were cut-off at 1.1 nm.

The trajectories were saved every nanosecond, generating 4001 frames (4 μs) for each simulation.

Analyses of the Coarse-Grained Simulations

For each system, the 1% of the all generated structures (1% of 4001 frames*1000 simulations = 40.010 frames in total) with the lowest protein–protein interaction energy (defined as the sum of the Lennard-Jones and Coulomb interactions) were extracted and combined into a single trajectory.

After removing the periodic boundary conditions and centering the proteins in the box, the trajectory was further processed by fitting both translational and rotational movements of the first protein (e.g., in the hetero-dimer case, the Mcl-1 was fitted). The trajectory has been then clustered using the Gromos algorithm (19) based on the root mean square deviation (RMSD) distance of the dimers. The least-squares fit and RMSD calculation are based on the whole dimer structure. The RMSD distance between two clusters was set to 0.2 nm (RMSD cut-off). For the first five most populated clusters (containing > 95 % of the whole structures), the contact occupancy, averaged by all the structures within the same cluster, have been calculated using the gmx mindist tool and in-house Python scripts. Two amino acids were considered to be in contact if any of their atoms were closer than 0.6 nm. The most representative structure (as the centroid of the structures in a given cluster) of the first two most populated clusters showing a different dimerization motif have been chosen to be fine-grained and tested with atomistic details.

Atomistic Simulations

To study the stability of the dimers obtained from the coarse-grained simulations described above, we fine-grained the CG structures of the two most populated clusters (for each homo- and hetero-dimer), obtained from the clustering procedure described above, to the atomistic resolution using the CHARMM-GUI (4). Atomistic dimers were subsequently embedded in the lipid bilayers containing 150 POPC molecules. For a given dimer, three independent starting structures (repetitions) have been prepared using the CHARMM-GUI (4) membrane builder. All simulated systems were explicitly solvated by 6000 water molecules (corresponding to a 40:1 water/lipid ratio), and counter ions were added to neutralize the systems. Each system was energy minimized and equilibrated for 100 ns, first with the position restraints on the peptide's heavy atoms and then on backbone atoms. Finally, all restrains were released and systems were subjected to 1 μs of the production run. The whole production run trajectory has been used for analysis. The final frames of the Mcl-1 / Mcl-1 homodimer and Mcl-1 / Bok heterodimer were used to introduce single point mutations using MODELLER 9 [DOI: 10.1002/cpbi.3, DOI:

10.1146/annurev.biophys.29.1.291, DOI: 10.1006/jmbi.1993.1626, Doi: 10.1110/ps.9.9.1753]. Each system was energy minimized with position restraints on the peptide's heavy atoms and then simulated for 1 μs. See **Table 2** for simulations details.

Table 2. Details on the atomistic simulations.

Monomer simulations				
Dimer	# POPC	# Water	Time (μs)	# Repeats
Mcl-1	128	5120	1	1
Bok	128	5120	1	1
Bax	128	5120	1	1
Mcl-1 - G340P	128	5120	1	1
Wild type dimer simulations				
Mcl-1 / Mcl-1	150	6000	1	6*
Bok / Bok	150	6000	1	6*
Bax / Bax	150	6000	1	6*
Mcl-1 / Bok	150	6000	1	6*
Mcl-1 / Bax	150	6000	1	6*
Mutated homodimer simulations				
Mcl-1- G340P / Mcl-1-G340P	150	6000	1	6*
Mcl-1- G344I / Mcl-1-G344I	150	6000	1	6*
Mcl-1- A339T / Mcl-1-A339T	150	6000	1	6*
Mcl-1- L348V / Mcl-1-L348V	150	6000	1	6*

Mutated heterodimer simulations				
Mcl-1- G340P / Bok	150	6000	1	6*
Mcl-1- G344I / Bok	150	6000	1	6*
Mcl-1- A339T / Bok	150	6000	1	6*
Mcl-1- L348V / Bok	150	6000	1	6*
Mcl-1- G340P / Bax	150	6000	1	6*
Mcl-1- G344I / Bax	150	6000	1	6*
Mcl-1- A339T / Bax	150	6000	1	6*
Mcl-1- L348V / Bax	150	6000	1	6*

* We fine-grained the CG structures of the two most populated clusters. For each cluster, we ran three independent simulations 1 us long.

The atomistic simulations were performed with GROMACS 2018.2 package (13) using the CHARMM36 force field for peptides (6) and lipids (5). The CHARMM-specific TIP3P model for water was employed. These models are the same that were employed in the aforementioned atomistic simulations used to relax the peptide monomers, and the simulation setup described below also holds for these relaxation simulations. All simulations were performed under isothermic-isobaric (NpT) ensemble with the time step of 2 fs. The Nosé-Hoover thermostat (14,15) with a time constant of 1 ps was used to maintain the constant temperature of 310 K. The temperature of peptides, lipids, and solvent were controlled independently. The Parrinello-Rahman barostat (16) with the time constant of 5 ps was utilized to keep the pressure the system at 1 bar. A semi-isotropic scheme was used for pressure control. The Verlet cutoff scheme (17) was employed. The electrostatic interactions were calculated using particle mesh Ewald (PME) method (20) with the cutoff at 1.2 nm. The Lennard-Jones interactions were cut off at 1.2 nm. The SETTLE (21) and LINCS (22) algorithms were used to constrain the geometry of the water molecule and bonds involving hydrogen atoms, respectively.

Analyses of the Atomistic Simulations

The RMSD of the peptides was calculated using the GROMACS tool, gmx rms. To describe the orientation of the peptides inside the lipid bilayer, two angles were used. The overall tilt angle of the dimer, indicating the tilt of the dimer as a whole with respect to the bilayer normal, was defined as the angle between a vector connecting the top (the center of mass of the top four residues from each monomer) and the bottom (the center of mass of the bottom four residues from each

monomer) of the dimer and the z axis (bilayer normal). The crossing angle, describing the mutual orientation of the monomers, was defined as the angle between the two vectors connecting the top (the center of mass of the top four residues) and the bottom (the center of mass of the four bottom residues) of each monomer. Both angles were calculated using in-house Python scripts. The alpha-helical content of the peptides was evaluated using the gmx do_dssp and DSSP (23) tools. Numbers of contacts between each amino acid in the dimer have been calculated using gmx mindist tool. Two amino acids were considered to be in contact if any of their atoms were closer than 0.6 nm. This analysis has been repeated with the cut-off of 0.4 nm. Contact occupancy equal 1.0 corresponds to the situation where given amino acids were in contact all the time.

The input files to reproduce our simulations can be found here:

1) Monomeric Simulations:

https://doi.org/10.5281/zenodo.4012224

2) Dimerization Simulations:

https://doi.org/10.5281/zenodo.4022900

References

1. T. K. Kerppola, Bimolecular fluorescence complementation: visualization of molecular interactions in living cells. Methods in cell biology 85, 431-470 (2008).
2. Y. Kodama, C. D. Hu, An improved bimolecular fluorescence complementation assay with a high signal-to-noise ratio. BioTechniques 49, 793-805 (2010).
3. Y. Kodama, C. D. Hu, Bimolecular fluorescence complementation (BiFC) analysis of protein-protein interaction: how to calculate signal-to-noise ratio. Methods in cell biology 113, 107-121 (2013).
4. J. Lee et al., CHARMM-GUI Input Generator for NAMD, GROMACS, AMBER, OpenMM, and CHARMM/OpenMM Simulations Using the CHARMM36 Additive Force Field. Journal of chemical theory and computation 12, 405-413 (2016).
5. J. B. Klauda et al., Update of the CHARMM all-atom additive force field for lipids: validation on six lipid types. The journal of physical chemistry. B 114, 7830-7843 (2010).
6. J. Huang, A. D. MacKerell, Jr., CHARMM36 all-atom additive protein force field: validation based on comparison to NMR data. Journal of computational chemistry 34, 2135-2145 (2013).
7. N. Eyal, Simulation of activation free energies in molecular systems. J. Chem. Phys. 105, 1902 (1996).
8. R. M. Venable, Y. Luo, K. Gawrisch, B. Roux, R. W. Pastor, Simulations of anionic lipid membranes: development of interaction-specific ion parameters and validation using NMR data. The journal of physical chemistry. B 117, 10183-10192 (2013).
9. S. J. Marrink, D. P. Tieleman, Perspective on the Martini model. Chemical Society reviews 42, 6801-6822 (2013).
10. M. Javanainen, H. Martinez-Seara, I. Vattulainen, Excessive aggregation of membrane proteins in the Martini model. PloS one 12, e0187936 (2017).
11. T. A. Wassenaar et al., High-Throughput Simulations of Dimer and Trimer Assembly of Membrane Proteins. The DAFT Approach. Journal of chemical theory and computation 11, 2278-2291 (2015).
12. M. Javanainen, Universal Method for Embedding Proteins into Complex Lipid Bilayers for Molecular Dynamics Simulations. Journal of chemical theory and computation 10, 2577-2582 (2014).
13. M.J. Abraham *et al.*, GROMACS: High performance molecular simulations through multi-level parallelism from laptops to supercomputers. *Software X*, 1-2 **19** (2015).
14. S. Nosé, A unified formulation of the constant temperature molecular dynamics methods. *J. Chem. Phys.* **81**, 511 (1984).
15. W.G. Hoover, Canonical dynamics: Equilibrium phase-space distributions. *Phys Rev A Gen Phys*. **31(3)**, 1695-1697 (1985).
16. M. Parrinello *et al*., Polymorphic transitions in single crystals: A new molecular dynamics method. *J. Appl. Phys.* **52,** 1463 (1981).

17. S. Páll, B. Hess, A flexible algorithm for calculating pair interactions on SIMD architectures. *Comput. Phys. Commun.* **184**, 2641 (2013).
18. D.H. De Jong *et al.*, Martini straight: boosting performance using a shorter cutoff and GPUs. *Comput. Phys. Commun.* **199**, 1 (2016).
19. Daura X., Peptide folding: when simulation meets experiment. *Angew. Chemie Int.* Ed. **38,** 236 (1999).
20. U. Essmann *et al.*, A smooth particle mesh Ewald method. *J. Chem. Phys.* **103,** 8577 (1995).
21. S. Miyamoto *et al.*, Settle: An analytical version of the SHAKE and RATTLE algorithm for rigid water models. *J. Comput. Chem.* **13**, 952 (1992).
22. B. Hess *et al.*, LINCS: a linear constraint solver for molecular simulationsJ. *Comput. Chem.* **18**, 1463 (1997).
23. W. Humphrey *et al.*, VMD: visual molecular dynamics. *J. Mol. Graph.* **14,** 33(1996).

Table S1. The average helical content (in percentage) of each monomer from homo- and hetero-dimers. The average is calculated over time and for three repetitions for each system.

System	Mcl-1-Mcl-1		Bok-Bok		Bax-Bax		Mcl-1-Bok		Mcl-1-Bax*	
	Mcl-1 monomer	Mcl-1 monomer	Bok monomer	Bok monomer	Bax monomer	Bax monomer	Mcl-1 monomer	Bok monomer	Mcl-1 monomer	Bax monomer
Cluster1	89 %	89 %	71 %	79 %	83 %	84 %	88 %	80 %	-	-
Cluster2	90 %	88 %	73 %	75 %	73 %	85 %	85 %	82 %	-	-

*majority of the time dimers were dissociated.

Table S2. The average overall tilt (in degrees) of the dimer with respect to the bilayer normal. The average is calculated over time and for three repetitions for each system.

System	Mcl-1-Mcl-1	Bok-Bok	Bax-Bax	Mcl-1-Bok	Mcl-1-Bax *
Cluster1	20.3	25.0	14.8	24.0	-
Cluster2	8.6	21.4	11.2	12.0	-

*majority of the time dimers were dissociated.

Table S3. The average crossing angle (in degrees) between the monomers forming the dimer. The average is calculated over time and for three repetitions for each system.

System	Mcl-1-Mcl-1	Bok-Bok	Bax-Bax	Mcl-1-Bok	Mcl-1-Bax *
Cluster1	25.9	17.1	18.4	23.6	-
Cluster2	45.2	24.1	19.1	62.0	-

*majority of the time dimers were dissociated.

Table S4. Somatic mutations of Mcl-1 TMD obtained from COSMIC database

Protein	Mutation	Pathogenic score	Tissue	Primary histology	PMID
Mcl-1	A339T	0.93		Malignant melanoma	24265153
	L348V	0.79	Lung	Adenocarcinoma	22980975

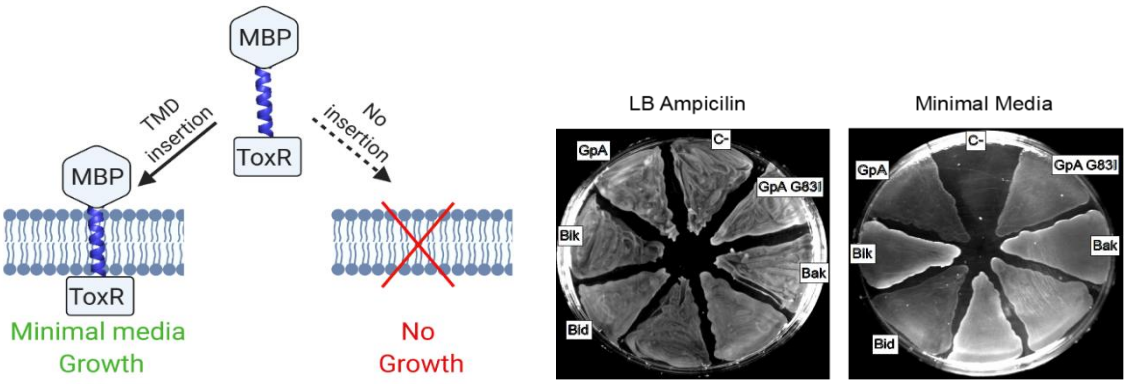

Figure S1. Membrane insertion of TMD controls in the ToxR system. Maltose complementation assay to test ToxR-TMD-MBP chimera topology in Bcl-2 TMD constructs. MM39 cells, lack endogenous Maltose Binding Protein (MBP), and consequently are unable to grow on minimal media with maltose as carbon source. If the ToxR-TMD-MBP constructs are correctly inserted in the inner membrane, will complement the MM39 *malE*-deficient phenotype and support growth on maltose. MalE-deficient E. coli MM39 transformed with the different ToxR-TMD-MBP constructs were cultured on either on complete medium LB (Left) or M9 agar containing 0.4% maltose (Right).

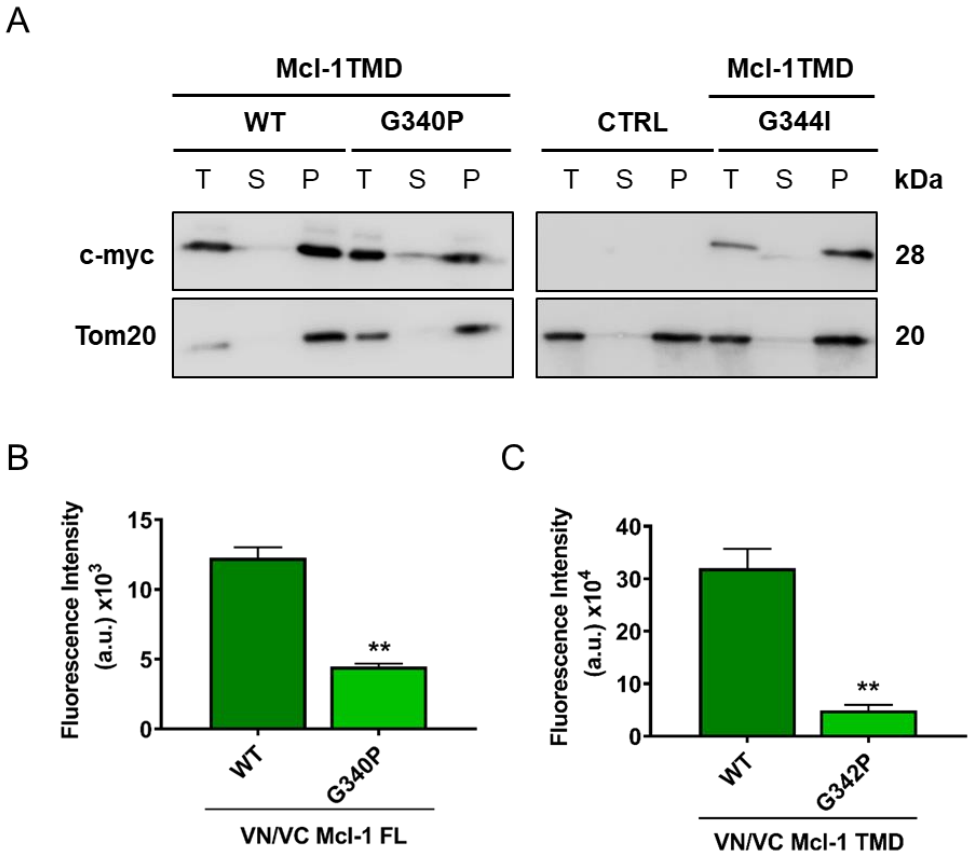

Figure S2. Mitochondrial membrane insertion of Mcl-1 TMD mutants. (A) Alkaline carbonate extraction of HCT116 cell mitochondria expressing the different Mcl-1 TMD mutants. Mitochondrial fraction was controlled using Tom20. Proteins were directly extracted with detergent (total, T), or treated with sodium carbonate solution (pH 11.5) to remove loosely attached membrane proteins (soluble fraction, S; membrane proteins, P). **(B)** Oligomerization analysis of the VN and VC Mcl-1 FL WT and G340P mutant measured by BiFC in HCT116 cells. **(C)** Oligomerization analysis of the Mcl-1 WT TMD and single amino acid G342P TMD mutant measured by BiFC in HCT116 cells. Error bars represent the mean ± SEM, n = 4. P-value, according to Dunnett's test, displayed. **P < 0.01.

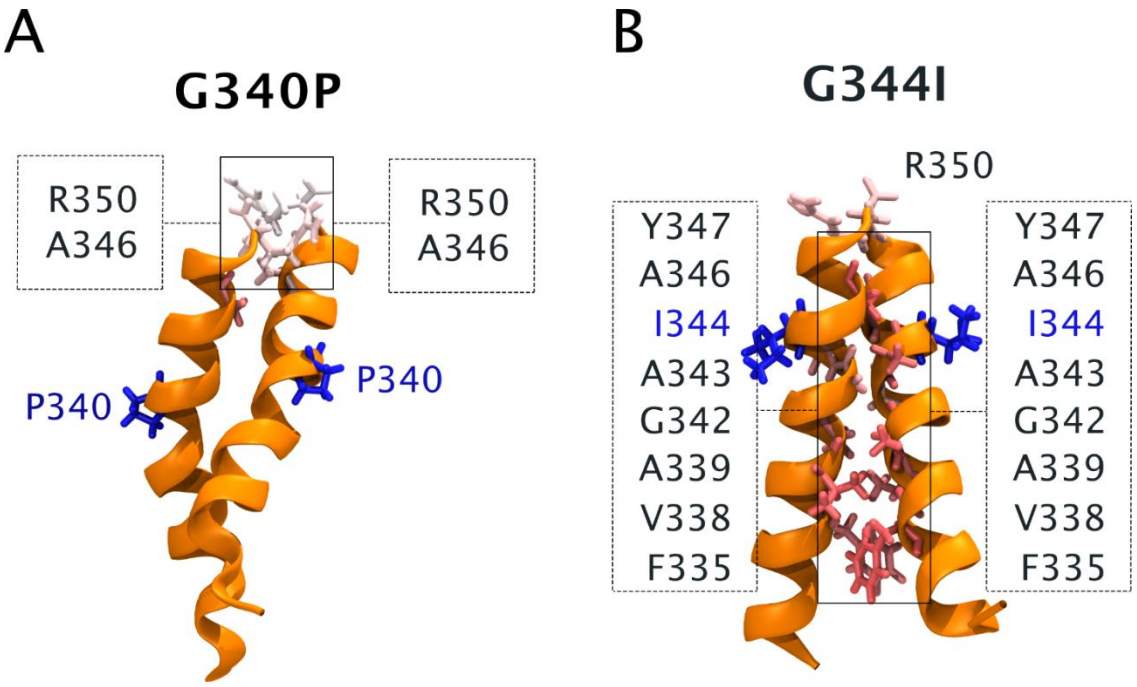

Figure S3. Homodimers of Mcl-1 mutants from molecular dynamics simulations. (A) Mcl-1 G340P and **(B)** Mcl-1 G344I homodimer average structure based on Mcl-1 Cluster2. Interfaces are shown illustrating the contribution to the interaction for each residue with a contribution > 0.5. This is defined as the sum of the occupancy of contacts for each residue normalized to the maximum value within all systems and is represented with the colored licorice draw method using the blue-white-red color scale, where red indicates large values.

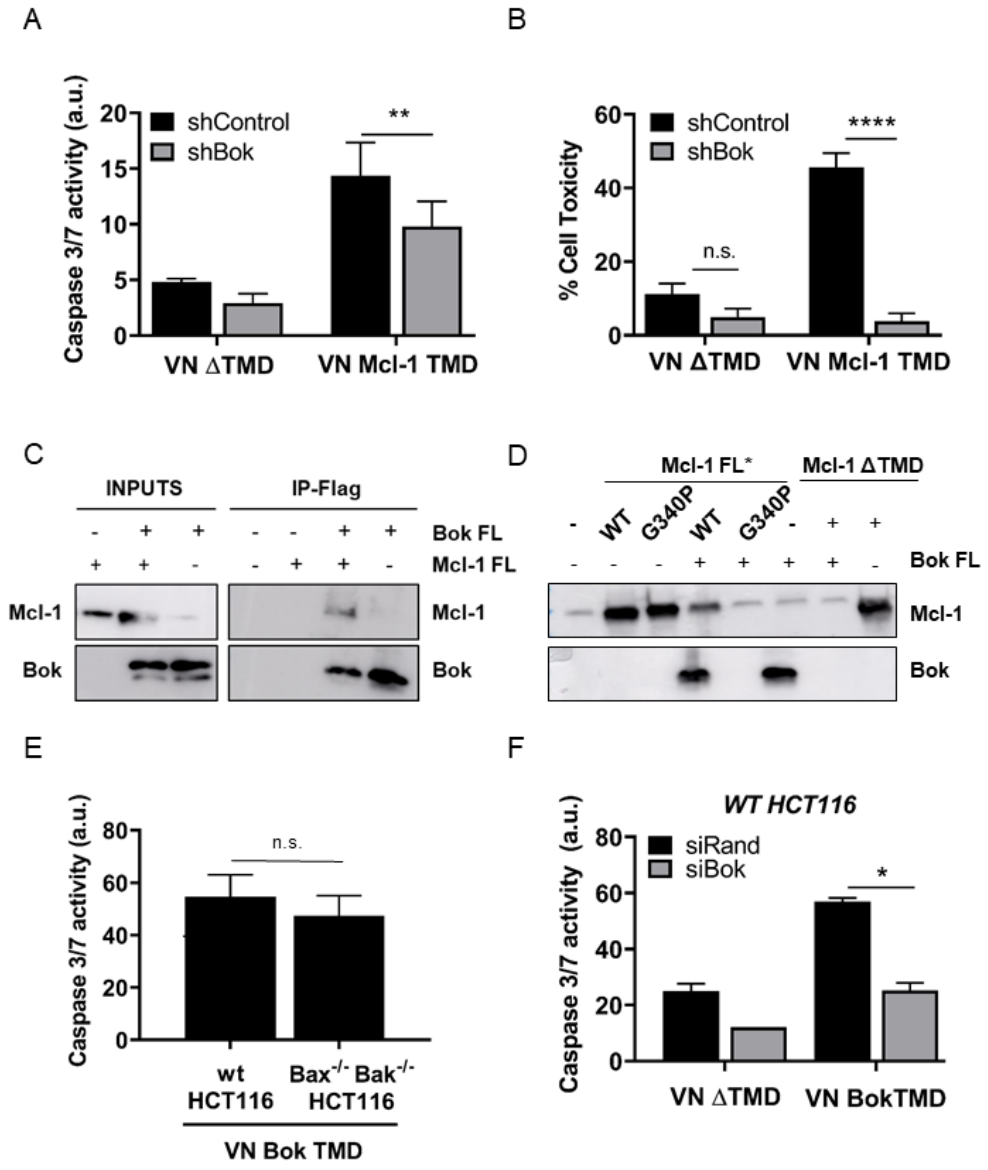

Figure S4. Mcl-1 TMD and Bok TMD cell death induction depend on Bok. Caspase 3/7 activity **(A)** and cell toxicity **(B)** of HCT116 cells transfected with VN Mcl-1 TMD in HCT116 shControl and shBok cells. Error bars represent the mean ± SEM, n = 3 (**P < 0.01; ***P < 0.001)**. (C)** Flag-Bok FL and the Mcl-1 FL were co-expressed in HCT116 cells. Immunoprecipitates were analyzed by Western blotting with anti-Bok and anti-Mcl-1 antibodies. **(D)** Immunoblotting of HCT116 extracts transfected with Mcl-1 TMD or Mcl-1 FL (WT, G340P mutant or ΔTMD) in the presence of Bok FL when indicated. **(E)** Caspase 3/7 activity was analyzed in WT and $Bax^{-/-}$ $Bak^{-/-}$ HCT116 cells transfected with the VN Bok TMD. **(F)** Caspase 3/7 activity was measured in HCT116 cells transfected with the VN Bok TMD or VN ΔTMD after 24 h of Bok silencing (siRNA Bok, siBok; siRNA Random, siRand). Error bars represent the mean ± SEM, n = 3. P-value, according to Sidak's test, displayed. *P < 0.05.

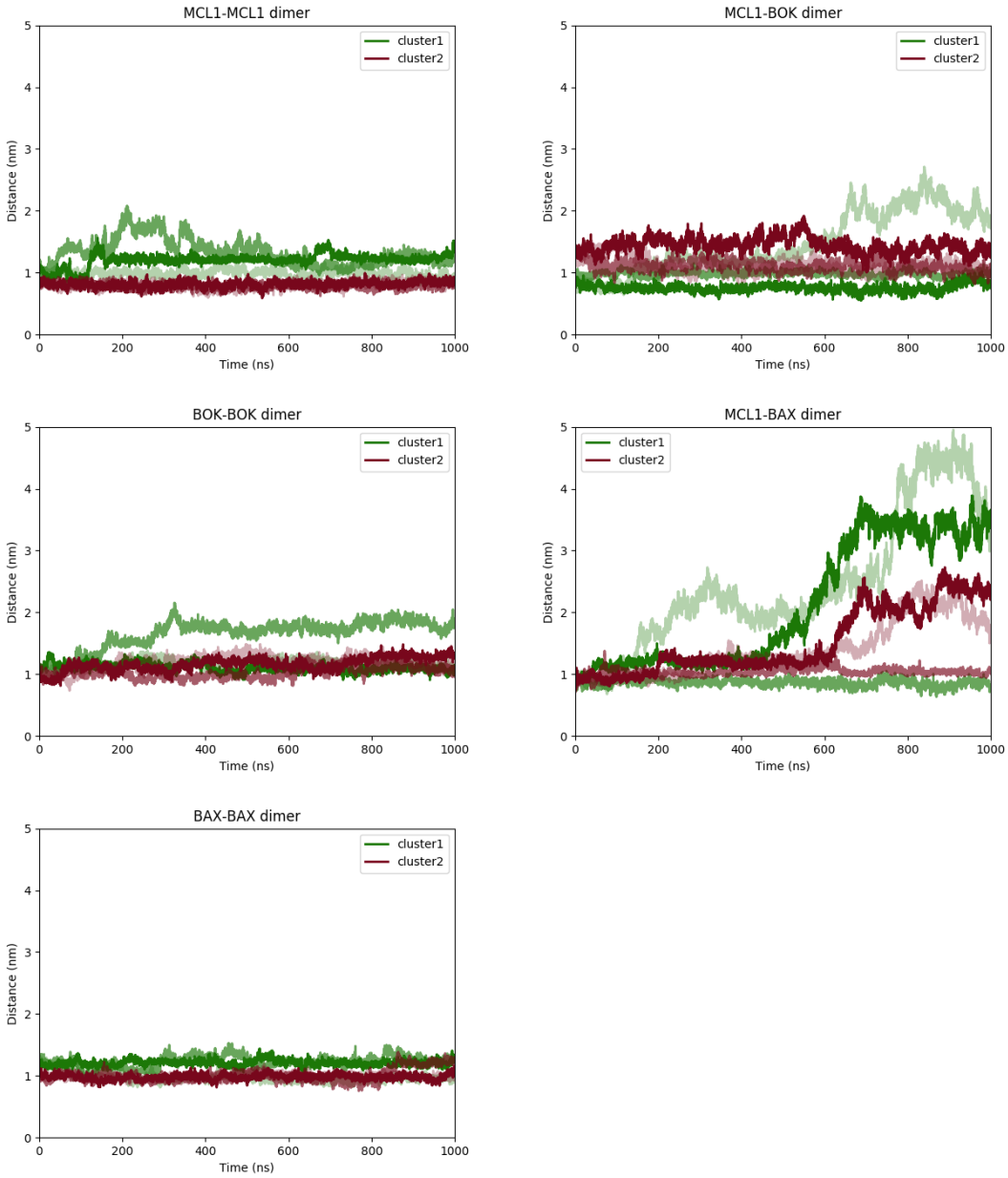

Figure S5. Time Evolution of Distance between the Centers of Mass of each Monomer. Different shades of green and red correspond to three repetitions of each cluster.

Differences in Mcl-1/Bok and Mcl-1/Bax interacting interfaces

We calculated the amino acid–amino acid contact occupancies to elucidate the differences in the heterodimer interactions between Mcl-1 and Bok/Bax. Several Bok residues (V192, L195, L202, and F206) are strongly involved in the heterodimer interactions stabilizing the Mcl-1/Bok interface (Figure S6A, top). On the other hand, the Mcl-1/Bax interface is less stable as indicated by lower amino acid–amino acid contact occupancies. In the case of Mcl-1/Bax interface, there are couple of shallow minima (Figure S6 B, bottom), with the interaction energies not lower than -6 kJ/mol. However, in the case of the Mcl-1/Bok interface, much deeper interaction energy minima are observed (Figure S6A, bottom).

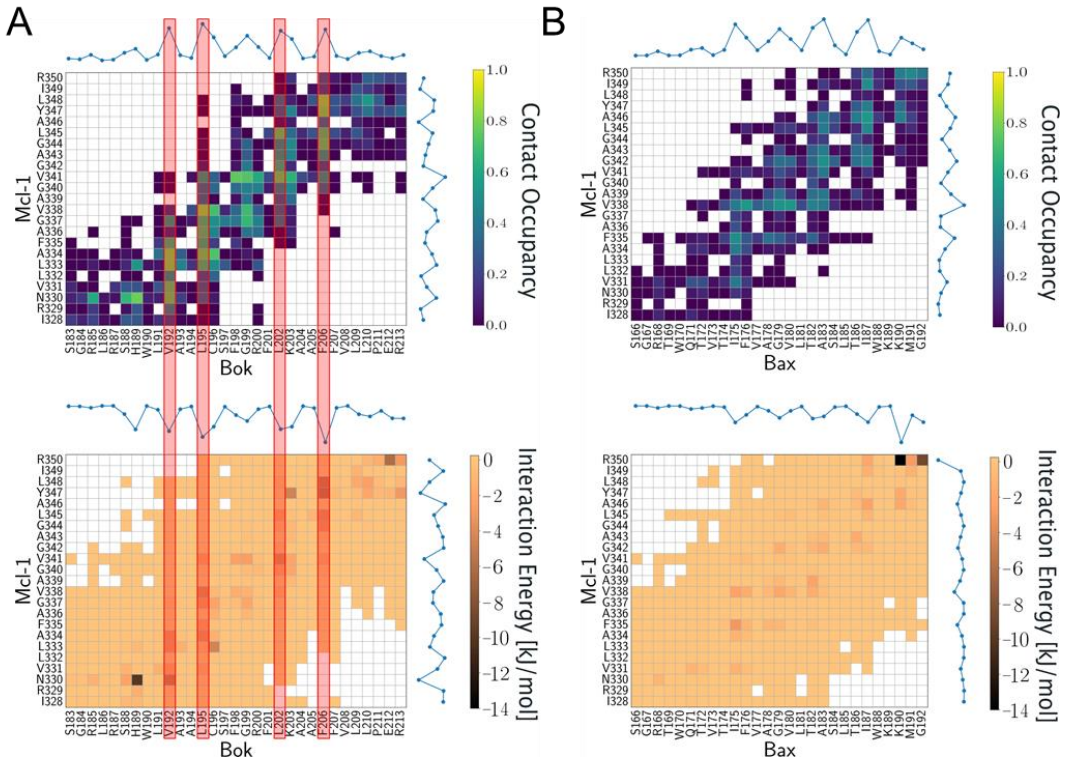

Figure S6. (A) (Top) The average amino acid–amino acid occupancies of contact and (Bottom) average interaction energy of each residue pair in Mcl-1/Bok heterodimer. Two amino acids were considered to be in contact if any of their atoms were closer than 6 Å. The blue line on the top and right shows the sum of contacts/interaction energies in the column and row, respectively. **(B)** The average amino acid–amino acid occupancies of contact and (Bottom) and average interaction energy of each residue pair in Mcl-1/Bak heterodimer.

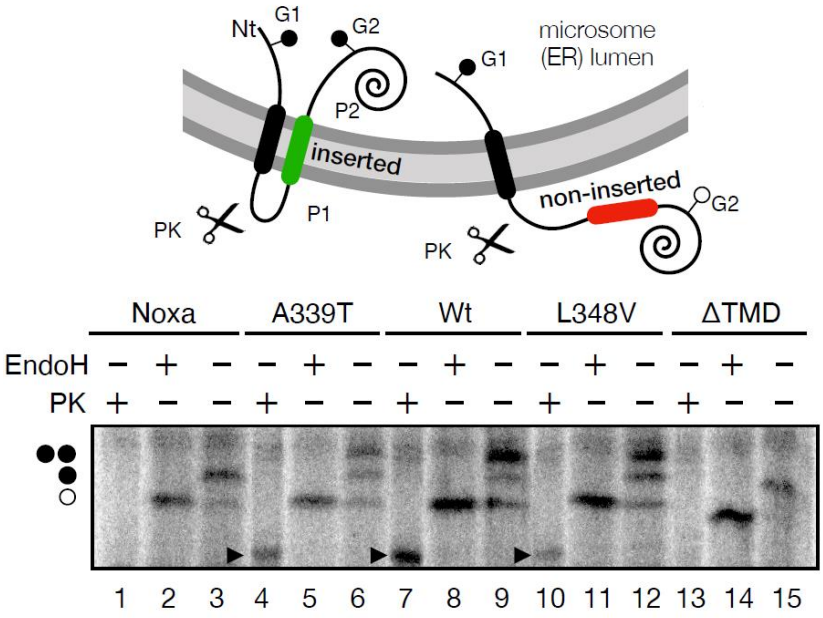

Figure S7. Somatic mutations in Mcl-1 TMDs do not affect insertion capability. (Top) Schematic of the engineered leader peptidase (Lep) model protein to analyze insertion of Mcl1 TMD patient mutations into microsomal membranes. The Mcl1 TMD related sequences (colored) were engineered into the luminal P2 domain and are flanked by two artificial glycosylation acceptor sites (G1 and G2) for N-linked glycosylation. Double glycosylation (i.e., membrane insertion, left) results in a molecular mass increase of ~5 kDa relative to the observed molecular mass of Lep; the molecular mass shifted ~2.5 kDa upon single glycosylation (i.e. non-insertion, right). The nature of these higher molecular weight polypeptide species was analyzed by endoglycosidase H (EndoH) treatment, a highly specific enzyme that cleaves N-linked oligosaccharides regardless of their location. Proteinase K (PK) added to microsomal vesicles will digest the outer microsomal membrane exposed, P1 domain to produce a protected TMD/P2 fragment when the P2 domain is located in the lumen of the microsomes (left). (Bottom) *In vitro* protein translation in the presence of rough microsomes, radiolabeled amino acids and in the presence (+) or absence (–) of EndoH (lanes 2, 5, 8, 11 and 14) or PK (lanes 1, 4, 7, 10 and 13). Translation products were ultracentrifuged on a sucrose cushion and analyzed by SDS-PAGE. Non-glycosylated protein bands are indicated by a white dot; single and double glycosylated protein bands are indicated by one or two black dots, respectively. A black triangle indicates protected glycosylated TMD/P2 fragments. The C-terminal region of Noxa (lanes 1-3) and a Lep version with the second TMD deleted (lanes 13-15) were included as a non-inserting controls (Andreu-Fernández V, et al. (2016) The C-terminal Domains of Apoptotic BH3-only Proteins Mediate Their Insertion into Distinct Biological Membranes. J.Biol.Chem. 291(48):25207–25216).

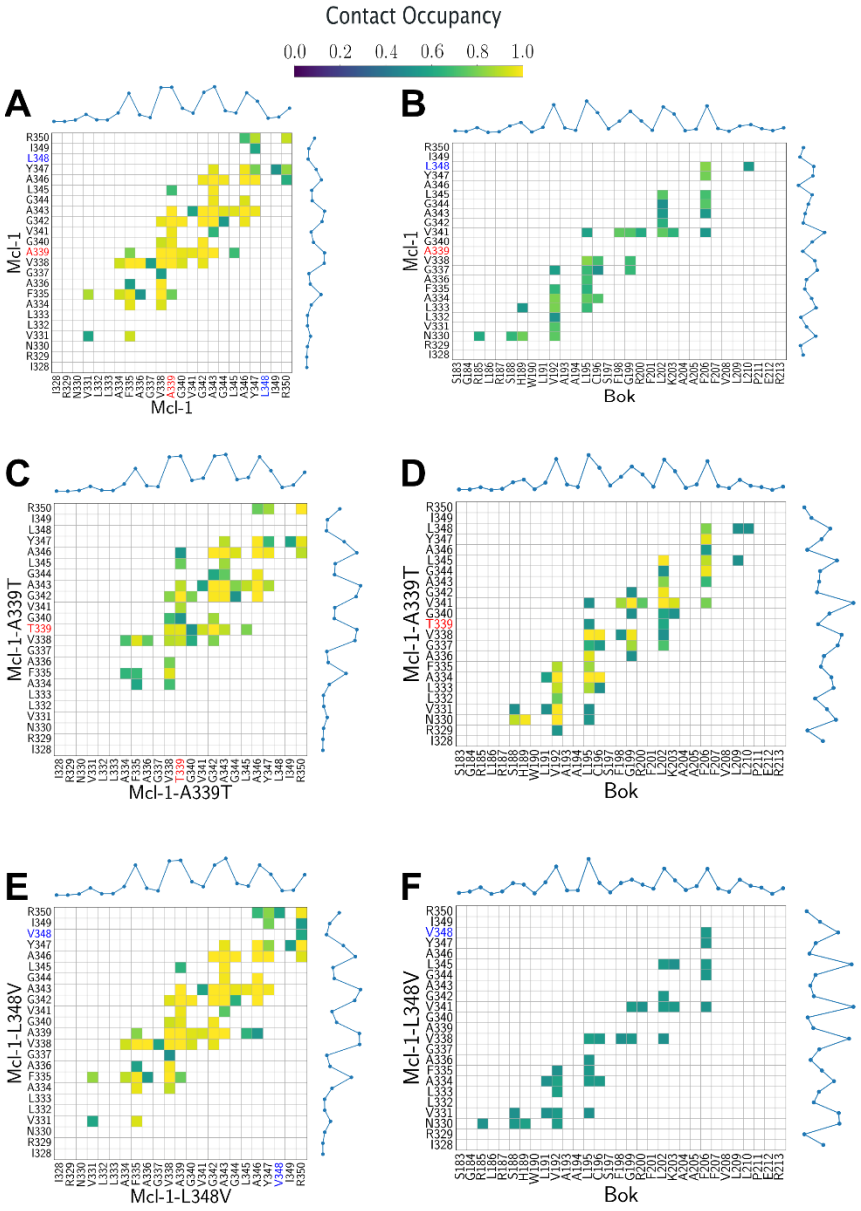

Figure S8. Amino acid–amino acid contact occupancies in the Mcl-1/Mcl-1 and Mcl-1/Bok dimers, including both Mcl-1 wild type and its patient's mutations (Mcl-1-A339T and Mcl-1-L348V). Figure S11 A (Mcl-1/Mcl-1 homodimer), shows the interaction interface is highly symmetrical, and the key residues are involved in multiple contacts between both monomers. It indicates that a single mutation in Mcl-1 / Mcl-1 homodimer will have a more substantial effect than the respective Mcl-1 / Bok heterodimer since the mutation is affecting both monomers. This assumption is confirmed in the case of Mcl-1-A339T / Mcl-1-A339T and Mcl-1-A339T / Bok dimers. Figures S5 C-D are indeed showing that a punctual mutation of residue A339, which is strongly involved, based on our simulations, in the homodimer formation (Figure S11 A), destabilizes the homodimer interaction interface weakening all network of contacts (Figure S11 C). In the case of Mcl-1/ Bok heterodimer, residue A339 is not involved in the interaction interface (Figure S11 B) and its mutation, instead, strength the interaction interface making new contacts

with Bok resulting in a higher number of contacts respect to the wild type heterodimer (Figure S11 B). Our simulations, however, are not able to let us make a similar conclusion for the Mcl-1-L348V case (Figure S11 E-F) which residue L348 is not participating in the homodimer formation (Figure S11 A). As mutations at the ends of the transmembrane helices are more affected by the interfacial effect of lipids, predictions from in silico modeling could be less accurate.

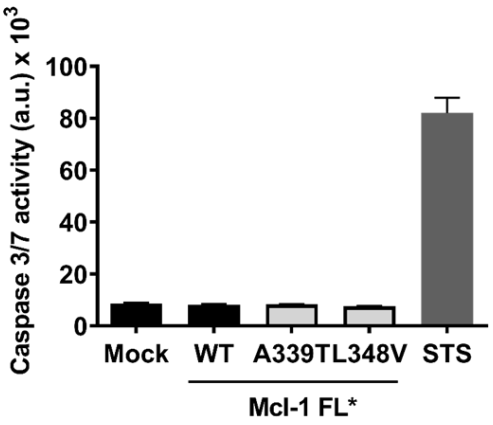

Figure S9. Introduction of somatic mutations in Mcl-1 FL does not alter caspase 3/7 activity. Caspase 3/7 activity induced by Mock plasmid, Mcl-1 WT FL, or mutant FL was analyzed in cytosolic extracts from HCT116 cells 16 h after transfection. Staurosporine (STS; 100 nM) was used as a control for caspase induction. Error bars represent the mean ± SEM, n = 4.